Optics Letters

Miniature probe integrating optical-resolution photoacoustic microscopy, optical coherence tomography, and ultrasound imaging: proof-of-concept

Xianjin Dai,[1,†] Lei Xi,[3,†] Can Duan,[2] Hao Yang,[1] Huikai Xie,[2] and Huabei Jiang[1,3,*]

[1]Department of Biomedical Engineering, University of Florida, Gainesville, Florida 32611, USA
[2]Department of Electrical and Computer Engineering, University of Florida, Gainesville, Florida 32611, USA
[3]School of Physical Electronics, University of Electronic Science and Technology of China, Chengdu, China
*Corresponding author: hjiang@bme.ufl.edu

Received 20 March 2015; revised 27 May 2015; accepted 29 May 2015; posted 29 May 2015 (Doc. ID 236610); published 15 June 2015

In this Letter, we present a novel tri-modal miniature side-view probe, through which optical-resolution photoacoustic microscopy (OR-PAM), optical coherence tomography (OCT), and pulse-echo ultrasound (US) images can be coaxially acquired and displayed simultaneously. The probe consists of a common optical path for OR-PAM (light delivery) and OCT (light delivery/detection), and a 40-MHz unfocused ultrasound transducer for OR-PAM (photoacoustic detection) and US (ultrasound transmission/receiving) with an overall diameter of 2 mm. Combining OR-PAM, OCT, and US would provide complementary information including optical absorption (OR-PAM), optical back-scattering (OCT), and deep tissue structures (US) about biological tissue. Based on an integrated imaging system consisting of OR-PAM, time-domain OCT, and US, phantom images and *in vivo* images of rat ear were acquired to demonstrate the capabilities of the integrated tri-modality imaging probe. The probe yields a lateral resolution of 13.6 μm for OR-PAM and OCT, and an axial resolution of 43 μm for OR-PAM and US. Currently, for a scanning area of 1 × 1 mm, it took ~25 min to acquire data for tri-modal volumetric imaging.

OCIS codes: (110.4190) Multiple imaging; (110.5120) Photoacoustic imaging; (110.4500) Optical coherence tomography; (110.7170) Ultrasound; (130.0130) Integrated optics; (180.0180) Microscopy.

http://dx.doi.org/10.1364/OL.40.002921

Photoacoustic microscopy (PAM) is an emerging noninvasive three-dimensional (3D) technique capable of imaging tissue absorption in high resolution [1–8]. In PAM, an image is formed through the detection of laser-induced ultrasound waves with an (un)focused ultrasound transducer. Since hemoglobin molecules are strong optical absorbers within a unique range of optical spectrum, PAM is ideal for mapping vasculatures in biological tissue through using light with a specific wavelength (such as 532 nm). Optical coherence tomography (OCT) is a widespread imaging technique by measuring back-scattered or back-reflected light generated from a light source delivered to the examined tissue, which is able to provide optical properties of tissue with a high resolution. While OCT is ideal for imaging retina [9], it has also been used to visualize other tissues [10–12]. Thus, through combining PAM and OCT, both optical absorption and back-scattering information can be obtained. In this regard, we and other groups have made efforts to develop an integrated platform combining PAM and OCT [13,14]. These studies have demonstrated the advantages of a dual-modality system. For example, for *in vivo* microcirculation studies, PAM provided absorbing components such as blood vessels, while OCT obtained the fine structures of the surrounding tissues.

Since pulse-echo ultrasound (US) can image deep tissue structures and a common ultrasound transducer can be used for both US and PAM, these two modalities have recently been combined as another dual-modality approach [15–17]. Among these PAM and US dual-modal studies, Bai *et al.* [15] reported a probe with an overall diameter of 1.1 mm, representing the smallest in size in PAM and US combinations.

It is conceivable that a tri-modal approach combining PAM, OCT, and US would provide a more powerful tool for tissue imaging. In this regard, Yang *et al.* [18] took an initial step toward the integration of three such modalities in a single probe by imaging ovarian tissue using OCT, US, and photoacoustic imaging (PAI). While this study is certainly inspiring, OCT, US, and PAI (where no focused light or transducer was used) were not physically integrated in a single probe. Moreover, PAI in their probe cannot visualize microvasculature due to its relatively poor resolution.

In this Letter, we present a tri-modal approach that integrates optical-resolution PAM (OR-PAM), OCT, and US in a single 2-mm-diameter probe. In this novel probe, OR-PAM

and OCT use the same optical path based on a single-mode fiber (SMF), a gradient index (GRIN) lens, and a thin gold-coated film, while OR-PAM and US share a 40-MHz unfocused ultrasound transducer, enabling these three modalities to coaxially obtain images from the same tissue volume. Both phantom and *in vivo* experiments were performed to demonstrate the capabilities of the integrated tri-modality imaging probe.

The schematic of the integrated miniature probe is shown in Fig. 1(a). In this probe, a single-mode fiber (SMF-28e+, Thorlabs) with a numerical aperture (NA) of 0.14 encapsulated by a ceramic ferrule (CFLC126-10, Thorlabs) with an outer diameter of 1.25 mm was used to deliver light for both OR-PAM and OCT. A custom-designed GRIN lens with a diameter of 0.7 mm and a working distance of 5 mm was used to focus the light beam from the tip of SMF with 8° angle facial cutting for minimizing back-reflection. The light beam was then reflected into the sample by a homemade thin gold-coated polyester film (48-1F-OC, CS Hyde Company, Illinois) with a thickness of 25 μm, attached to the tip of the stainless steel tubing (SST1) using epoxy glue. A custom-made unfocused ultrasound transducer with a center frequency of 40 MHz and a dimension of 0.6 × 0.5 × 0.2 mm (Blatek, Inc., State College, Pennsylvania) was mounted to the tip-wall of SST1. The ultrasound transducer should be placed coaxially with the optical path with respect to the thin film while fixing. The probe was protected by a second stainless-steel tubing (SST2) with an aperture opened at its tip to allow both light and ultrasound to transmit with minimal loss, which ultimately determined the overall size of the whole probe, i.e., 2.0 mm in diameter.

Compared to the conventional way of using 45° prism to reflect light and transmit ultrasound, here gold-coated film (GCF) was used to reflect light. Since the ultrasound attenuation caused by GCF was significantly smaller, it resulted in improved detection of both photoacoustic and ultrasound signals (in practice, the housing space between the transducer and GCF was filled with deionized water or the whole probe was immersed into a water tank). Further, the attenuation of GCF was quantitatively assessed by using the same ultrasound transducer as the probe and an ultrasound pulser/receiver (5073PR, Olympus) (as shown in Fig. 2). The ultrasound transducer (UST) and a steel plate (SP) were both placed in a water tank with a certain distance between each other. The echoes reflected by the steel plate were recorded with [Figs. 2(b) and 2(d)] and without [Figs. 2(a) and 2(c)] GCF between transducer and steel plate. By computing the ratio of peak-to-peak value of echoes with [Fig. 2(c), 0.45 V] and without (Fig. 2(d), 0.43 V) GCF, the two-way ultrasound attenuation caused by GCF was around 5%.

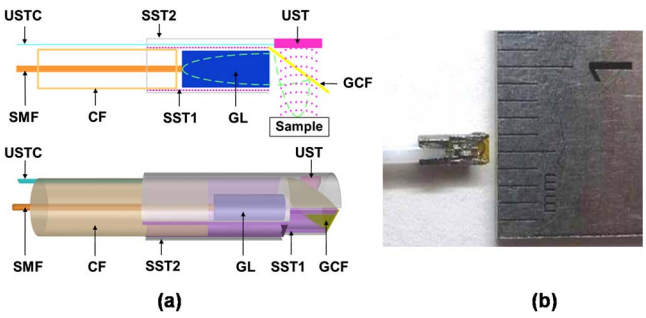

Fig. 1. Integrated probe. (a) Schematic and (b) photograph. GCF, gold-coated film; UST, ultrasound transducer; GL, gradient index lens; SST1–SST2, stainless-steel tubing; CF, ceramic ferrule; SMF, single-mode fiber; USTC, ultrasound transducer cable.

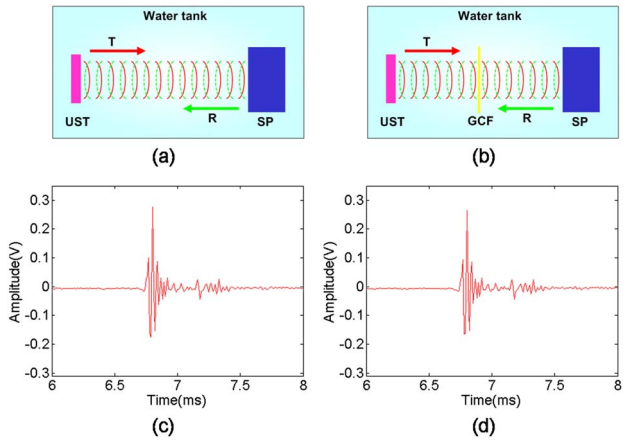

Fig. 2. Attenuation of gold-coated film (a) without and (b) with gold-coated film between ultrasound transducer and steel plate. (c) Echo of (a), (d) echo of (b). UST, ultrasound transducer; T, transmit wave; R, reflected wave; SP, steel plate; GCF, gold-coated film.

The integrated tri-modality imaging system is schematically shown in Fig. 3(a). The probe was mounted on a linear stage and immersed inside a water tank. A hole was drilled at the bottom of the water tank and sealed with transparent plastic film with a thickness of 50 μm to allow both light and ultrasound to transmit with minimized energy loss.

For OR-PAM and time-domain OCT, a nanosecond pulsed Nd:YAG laser having a repetition rate of 20 Hz and a center wavelength of 532 nm and a broadband light source with a full width at half maximum (FWHM) of 75 nm and a center wavelength of 1310 nm were used for OR-PAM and time-domain OCT, respectively. A data acquisition (DAQ) board (PCI-5124, National Instrument) with 12-bit resolution, a sampling

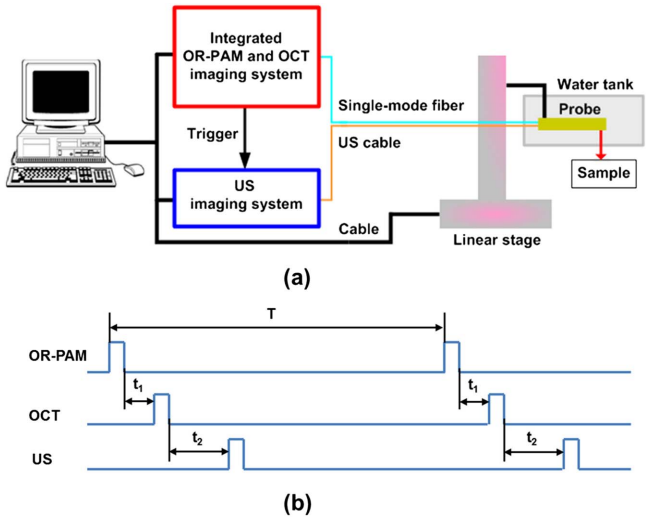

Fig. 3. Integrated tri-modality imaging system. (a) Schematic, (b) timing diagrams for synchronizing subsystems. T, 50 ms; t_1,10 μs; and t_2, 20 μs.

rate of 200 MS/s, and a signal-to-noise ratio (SNR) of 56 dB was used to resolve signals as small as 1 mV, enhancing the sensitivity of the data acquisition system. For US imaging, an ultrasound pulser/receiver (5073PR, Olympus) with an integrated amplifier and a bandwidth of 75 MHz, synchronized with OR-PAM/OCT, was used to generate ultrasound and receive echoes. By scanning in x–y plane with a two-dimensional (2D) linear stage, a volumetric image of sample could be obtained. Figure 3(b) shows the timing diagrams of the whole scanning, which is synchronized by the pulsed Nd:YAG laser with a repetition rate of 20 Hz (i.e., $T = 50$ ms). The signal acquisition of OR-PAM is triggered by the synchronizing output of pulsed Nd:YAG laser. With a 10-μs (t_1) delay, the time-domain OCT subsystem starts to collect signal. After 20 μs (t_2), US subsystem is triggered to acquire echoes from the sample. Currently, it takes around 25 min to acquire data for tri-modal volumetric imaging given a scanning area of 1 mm × 1 mm with a 6-μm step size, which is limited by the repetition rate of the pulsed laser (20 Hz) for OR-PAM.

The feasibility of the integrated tri-modality imaging system was first validated by experiments using a turbid tissue mimicking phantom [as shown in Fig. 4(a)]. The background of the phantom was composed of 2% Agar, TiO_2, and India ink with absorption coefficient of 0.007 mm^{-1} and reduced scattering coefficient of 1.0 mm^{-1}. Four simulated targets were used: (1) two pieces of human hair with a diameter of around 100 μm were embedded at a depth of 1.0 mm under the surface; (2) two pieces of bare optical fibers with a diameter of 0.4 mm were positioned with a depth of 2.0 mm. Figures 4(b) and 4(c) show the cross-sectional images of the phantom from OR-PAM and OCT, respectively. Both the OR-PAM and OCT images show clear boundary delineation of the hair at the depth of 1.0 mm, indicating the penetration depth of OR-PAM and OCT is more than 1.0 mm. Figure 4(d) gives the cross-sectional US image of the phantom, in which both the hair and bare fibers were detected, indicating the imaging depth of US is more than 2.0 mm. Figure 4(e) shows the overlap of tri-modal image through pseudo-RGB color coding with equal ratio of OR-PAM (R, red), OCT (G, green), US (B, blue), indicating the matched correlation of three modalities. Furthermore, through examining the images of the hair, it suggests that the spatial resolution of US is lower than OR-PAM and OCT. However, US imaging is able to image deeper targets.

The spatial resolution of OR-PAM was evaluated by imaging a carbon fiber with a diameter of 6 μm. Figure 5(a) shows the cross-sectional image of the carbon fiber. Figures 5(b) and 5(c), respectively, show the lateral and axial profiles corresponding to the dotted lines in Fig. 5(a). In Figs. 5(b) and 5(c), the dotted profile (blue) represents the experimental data, which is Gaussian fitted (red) indicating a lateral resolution of 13.6 μm and an axial resolution of 42.1 μm with a signal-to-noise ratio (SNR) of 28 dB. The axial resolution primarily depends on the bandwidth and central frequency of the ultrasound transducer, which is close to the axial resolution of 43.0 μm for US with a SNR of 32 dB estimated by using a tungsten wire with a diameter of 12 μm. We also used the same 6-μm-diameter carbon fiber to estimate the spatial resolution of OCT, which respectively gave a lateral resolution of 13.4 μm and an axial resolution of 14.3 μm with a SNR of 20 dB. The results suggest that both OR-PAM and OCT have similar lateral resolution determined by the point spread function of the light focus. Since the axial resolution of OCT is primarily determined by the FWHM of the light source, that 75 nm in our case resulting in an axial resolution of 10 μm.

To further demonstrate the potential clinical capabilities of this integrated tri-modal probe, *in vivo* imaging of a rat ear (rat weight = 70 g) was performed. Before the experiments, the hair on the ear was gently removed using a human-hair-removing cream. The rat was placed on a home-made animal holder and anesthetized by a solution of ketamine (85 mg/kg) and xylazine. The rat was sacrificed according to the University of Florida Institutional Animal Care and Use Committee (IACUC)-approved techniques after the experiments. Strict animal-care procedures approved by the University of Florida IACUC and based on guidelines from the National Institutes of Health (NIH) for the Care and Use of Laboratory Animals were followed. The laser exposure was about 15 mJ/cm^2 at the optical focus inside the ear tissue,

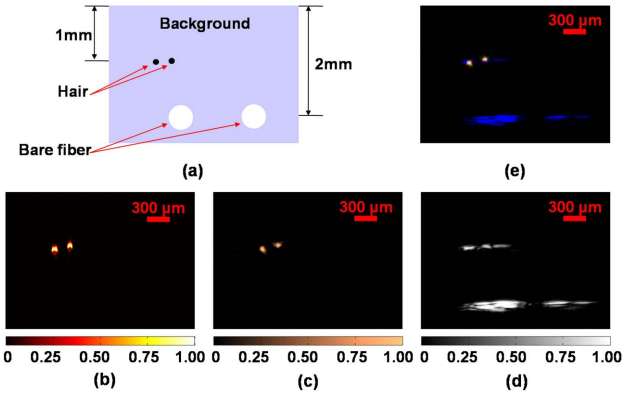

Fig. 4. Cross-sectional OR-PAM, OCT, and US images from tissue mimicking phantom. (a) Phantom geometry with four simulated targets, (b) OR-PAM image, (c) OCT image, (d) US image, (e) tri-modal color-coded RGB image.

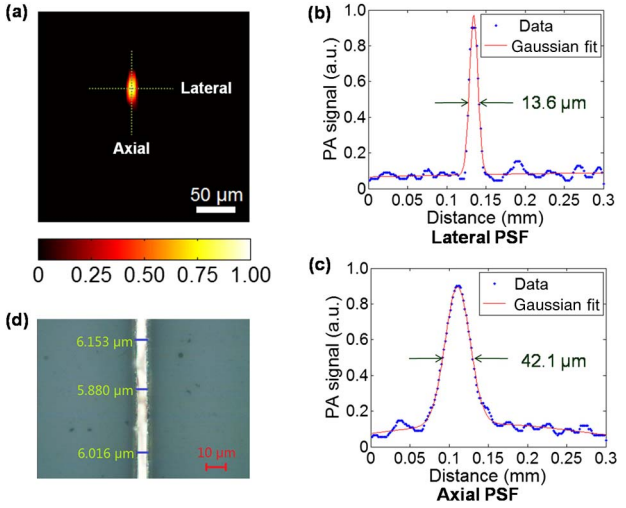

Fig. 5. Spatial resolution of OR-PAM. (a) OR-PAM cross-sectional image of a carbon fiber, (b) the lateral resolution, (c) the axial resolution, (d) high-resolution microscopy image of the carbon fiber. PSF, point spread function.

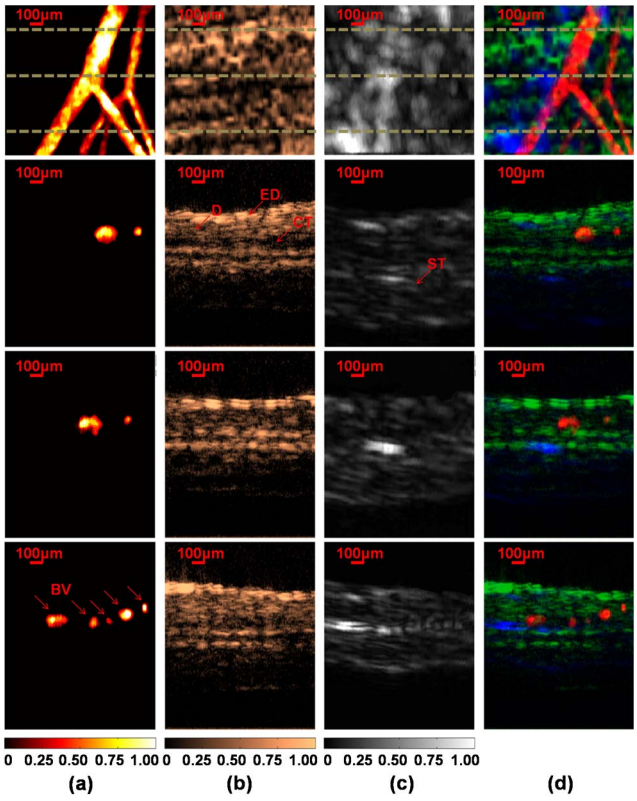

Fig. 6. *In vivo* imaging of a rat ear by the integrated tri-modality probe. Maximum amplitude projection (MAP) images (top row) and cross-sectional images (2nd, 3rd, and bottom rows) corresponding to the dotted lines shown in the MAP image of (a) OR-PAM, (b) OCT, (c) US, and (d) fused tri-modality. BV, blood vessel; ED, epidermis; D, dermis; CT, cartilage; ST, subcutaneous tissue.

which is lower than the American National Standards Institute (ANSI) laser safety limit (20 mJ/cm^2). The scanning step in the x–y plane was 6 μm, which is below the spatial resolution of our probe. The tri-modal images of a 1.2 × 1.2 mm area of the rat ear were obtained without average of the signals, taking around 36 min, which is limited by the repetition rate (20 Hz) of our pulse laser for OR-PAM.

The top row of Fig. 6 shows the maximum amplitude projection (MAP) images of OR-PAM [Fig. 6(a)], OCT [Fig. 6(b)], US [Fig. 6(c)], and fused tri-modal pseudo-color-coded RGB images [Fig. 6(d)] obtained with an equal ratio. The second, third, and bottom rows of Fig. 6 show the cross-sectional images of OR-PAM, OCT, US and fused tri-modality, corresponding to the three dashed lines in the respective MAP images.

We see that OR-PAM, OCT, and US, respectively, image the microvasculature, fine structures surrounding the blood vessels, and both superficial and deep tissue structures. To closely interpret these images, blood vessels in the rat ear are mapped by OR-PAM with the highest contrast [Fig. 6(a)], epidermis, dermis, and cartilage are identified by OCT [Fig. 6(b)], and deep tissues like subcutaneous tissue are visualized by US [Fig. 6(c)]. By overlapping the OR-PAM, OCT, US images [Fig. 6(d)], the structures/tissue morphology are better displayed.

In summary, we have developed a novel miniature probe which coaxially integrates OR-PAM, OCT, and US in a single platform, which is very suitable for *in vivo* imaging internal organs, such as endoscopic imaging and intravascular imaging. The phantom and *in vivo* experiments have shown that the tri-modal probe is able to offer high-resolution images of tissue absorption and optical back-scattering properties as well as deep tissue structures. For future studies, in order to enable broader potential applications of the integrated tri-modal probe with the imaging system, first, we need a rotary device to replace current bulky linear stage. A possible way is to implement an internal scanning mechanism based on micromotor. Second, currently, two lasers are used for OR-PAM and OCT, respectively, and thus the total cost is relatively high and the whole system is bulky. Moreover, the current imaging speed is mainly limited by the slow repetition rate (20 Hz) of the pulsed laser for OR-PAM. A high-repetition-rate pulsed laser with compact volume and low cost [such as diode-pumped solid-state (DPSS) laser with a repetition rate of 2–5 kHz] is required to both speed up imaging and reduce the whole volume and cost.

[†]These authors contributed equally to this work.

U.S. Department of Defense (DOD).

REFERENCES

1. A. De La Zerda, C. Zavaleta, S. Keren, S. Vaithilingam, S. Bodapati, Z. Liu, J. Levi, B. R. Smith, T.-J. Ma, and O. Oralkan, Nat. Nanotechol. **3**, 557 (2008).
2. Z. Xie, S. Jiao, H. F. Zhang, and C. A. Puliafito, Opt. Lett. **34**, 1771 (2009).
3. P. Hajireza, W. Shi, and R. Zemp, Opt. Lett. **36**, 4107 (2011).
4. Z. Xie, S.-L. Chen, T. Ling, L. J. Guo, P. L. Carson, and X. Wang, Opt. Express **19**, 9027 (2011).
5. R. Ma, S. Söntges, S. Shoham, V. Ntziachristos, and D. Razansky, Biomed. Opt. Express **3**, 1724 (2012).
6. B. Li, H. Qin, S. Yang, and D. Xing, Opt. Express **22**, 20130 (2014).
7. L. Xi, C. Song, and H. Jiang, Opt. Lett. **39**, 3328 (2014).
8. L. Yao, L. Xi, and H. Jiang, Sci. Rep. **4**, 4960 (2014).
9. J. G. Fujimoto, C. Pitris, S. A. Boppart, and M. E. Brezinski, Neoplasia **2**, 9 (2000).
10. B. Bouma, G. Tearney, H. Yabushita, M. Shishkov, C. Kauffman, D. D. Gauthier, B. MacNeill, S. Houser, H. Aretz, and E. Halpern, Heart **89**, 317 (2003).
11. D. C. Adler, C. Zhou, T.-H. Tsai, J. Schmitt, Q. Huang, H. Mashimo, and J. G. Fujimoto, Opt. Express **17**, 784 (2009).
12. T.-H. Tsai, J. G. Fujimoto, and H. Mashimo, Diagnostics **4**, 57 (2014).
13. S. Jiao, M. Jiang, J. Hu, A. Fawzi, Q. Zhou, K. K. Shung, C. A. Puliafito, and H. F. Zhang, Opt. Express **18**, 3967 (2010).
14. L. Xi, C. Duan, H. Xie, and H. Jiang, Appl. Opt. **52**, 1928 (2013).
15. X. Bai, X. Gong, W. Hau, R. Lin, J. Zheng, C. Liu, C. Zeng, X. Zou, H. Zheng, and L. Song, PLoS One **9**, e92463 (2014).
16. M. Gerling, Y. Zhao, S. Nania, K. J. Norberg, C. S. Verbeke, B. Englert, R. V. Kuiper, Å. Bergström, M. Hassan, and A. Neesse, Theranostics **4**, 604 (2014).
17. P. Subochev, A. Orlova, M. Shirmanova, A. Postnikova, and I. Turchin, Biomed. Opt. Express **6**, 631 (2015).
18. Y. Yang, X. Li, T. Wang, P. D. Kumavor, A. Aguirre, K. K. Shung, Q. Zhou, M. Sanders, M. Brewer, and Q. Zhu, Biomed. Opt. Express **2**, 2551 (2011).